arXiv:gr-qc/0603091v1 22 Mar 2006

Stable phantom energy traversable wormhole models

Francisco S. N. Lobo

Centro de Astronomia e Astrofísica da Universidade de Lisboa,
Campo Grande, Ed. C8 1749-016 Lisboa, Portugal

Abstract.
A possible candidate for the present accelerated expansion of the Universe is "phantom energy", which possesses an equation of state of the form $\omega \equiv p/\rho < -1$, consequently violating the null energy condition. As this is the fundamental ingredient to sustain traversable wormholes, this cosmic fluid presents us with a natural scenario for the existence of these exotic geometries. In this context, we shall construct phantom wormhole geometries by matching an interior wormhole solution, governed by the phantom energy equation of state, to an exterior vacuum at a junction interface. Several physical properties and characteristics of these solutions are further investigated. The dynamical stability of the transition layer of these phantom wormholes to linearized spherically symmetric radial perturbations about static equilibrium solutions is also explored. It is found that the respective stable equilibrium configurations may be increased by strategically varying the wormhole throat radius.

1. INTRODUCTION

One of the most challenging current problems in cosmology is explaining the accelerated phase of expansion of the Universe [1]. Several candidates, responsible for this cosmic expansion, have been proposed in the literature, namely, dark energy models, generalizations of the Chaplygin gas, modified gravity and scalar-tensor theories, tachyon scalar fields and braneworld models, such as the Dvali-Gabadadze-Porrati (DGP) model, amongst others. The dark energy models are parametrized by an equation of state given by $\omega = p/\rho$, where p is the spatially homogeneous pressure and ρ is the dark energy density. For the cosmic expansion, a value of $\omega < -1/3$ is required, as dictated by the Friedman equation $\ddot{a}/a = -4\pi(p+\rho/3)$, so that $\ddot{a} > 0$. A specific exotic form of dark energy, denoted phantom energy, has also been proposed, possessing the peculiar property of $\omega < -1$ [2]. This parameter range is not excluded by observation, and possesses peculiar properties, such as the violation of the null energy condition and an infinitely increasing energy density, resulting in a Big Rip, at which point the Universe blows up in a finite time [2]. However, recent fits to supernovae, CMB and weak gravitational lensing data indicate that an evolving equation of state ω crossing the phantom divide -1, is mildly favored [3].

As the phantom energy equation of state violates the null energy condition, $p+\rho < 0$, which is the fundamental ingredient to sustain traversable wormhole [4, 5], one now has at hand a possible source for these exotic spacetimes. However, a subtlety needs to be pointed out, as emphasized in Refs. [6, 7]. The notion of phantom energy is that of a homogeneously distributed fluid. When extended to inhomogeneous spherically symmetric spacetimes, the pressure appearing in the equation of state is now a radial pressure, and the transverse pressure is then determined via the field equations. Wormhole geometries were found in Ref. [6], by considering specific choices for the distribution of the energy density, and in Ref. [7], a complementary approach was traced out, by imposing appropriate choices for the form function and/or the redshift function, and the stress-energy tensor components were consequently determined. This latter approach shall be traced out in this paper.

It is also of a fundamental importance to investigate the stability of these phantom wormhole geometries. We shall model these spacetimes by matching an interior traversable wormhole geometry with an exterior Schwarzschild vacuum solution at a junction interface [8]. In this work, we analyze the stability of these phantom wormholes to linearized perturbations around static solutions. Work along these lines was done by considering thin-shell wormholes, using the cut-and-paste technique [9]. The advantage of this analysis resides in using a parametrization of the stability of equilibrium, so that there is no need to specify a surface equation of state. The stability analysis of these thin-shell wormholes to linearized spherically symmetric perturbations about static equilibrium solutions was carried out by

assuming that the shells remain transparent under perturbation [10]. This amounts to considering specific spacetimes that do not contribute with the momentum flux term in the conservation identity, which provides the conservation law for the surface stress-energy tensor. The inclusion of this term, corresponding to the discontinuity of the momentum impinging on the shell, severely complicates the analysis. However, we shall follow the approach of Ishak and Lake [10], with the respective inclusion of the momentum flux term and find stability equilibrium configurations of specific phantom wormhole geometries.

This paper is organized in the following manner. In Section 2, we outline the general properties of phantom energy traversable wormhole, and in Section 3, we present specific solutions of these phantom wormholes. We also show that using these specific constructions, and taking into account the "volume integral quantifier", one may theoretically construct these spacetimes with infinitesimal amounts of ANEC violating phantom energy. In Section 4, we outline a general linearized stability analysis procedure, and then apply this analysis to phantom wormhole geometries and determine their respective stability regions. Finally in Section 5, we conclude.

2. PHANTOM ENERGY TRAVERSABLE WORMHOLES

The spacetime metric representing a spherically symmetric and static wormhole is given by

$$ds^2 = -e^{2\Phi(r)}\,dt^2 + \frac{dr^2}{1-b(r)/r} + r^2\,(d\theta^2 + \sin^2\theta\,d\phi^2)\,, \tag{1}$$

where $\Phi(r)$ and $b(r)$ are arbitrary functions of the radial coordinate, r. $\Phi(r)$ is denoted as the redshift function, for it is related to the gravitational redshift; $b(r)$ is called the form function [4]. The radial coordinate has a range that increases from a minimum value at r_0, corresponding to the wormhole throat, to a, where the interior spacetime will be joined to an exterior vacuum solution.

Using the Einstein field equation, $G_{\hat{\mu}\hat{\nu}} = 8\pi T_{\hat{\mu}\hat{\nu}}$, in an orthonormal reference frame, (with $c = G = 1$) we obtain the following stress-energy scenario

$$b' = 8\pi r^2 \rho\,, \tag{2}$$

$$\Phi' = \frac{b + 8\pi r^3 p_r}{2r^2(1-b/r)}\,, \tag{3}$$

$$p_r' = \frac{2}{r}\,(p_t - p_r) - (\rho + p_r)\,\Phi'\,, \tag{4}$$

where the prime denotes a derivative with respect to the radial coordinate, r. $\rho(r)$ is the energy density, $p_r(r)$ is the radial pressure, and $p_t(r)$ is the lateral pressure measured in the orthogonal direction to the radial direction. Equation (4) may be obtained using the conservation of the stress-energy tensor, $T^{\mu\nu}{}_{;\nu} = 0$. At the throat we have the flaring out condition given by $(b - b'r)/b^2 > 0$ [4, 5], which may be deduced from the mathematics of embedding. From this we verify that at the throat $b(r_0) = r = r_0$, the condition $b'(r_0) < 1$ is imposed to have wormhole solutions. For the wormhole to be traversable, one must demand that there are no horizons present, which are identified as the surfaces with $e^{2\Phi} \to 0$, so that $\Phi(r)$ must be finite everywhere. Note that the condition $1 - b/r > 0$ is also imposed.

A fundamental ingredient of traversable wormholes and phantom energy is the violation of the null energy condition (NEC). Matter that violates the NEC is denoted as *exotic matter*. Note that the notion of phantom energy is that of a homogeneously distributed fluid; however, when extended to inhomogeneous spherically symmetric spacetimes, the pressure appearing in the equation of state is now a radial pressure, and the transverse pressure is then determined from Eq. (4). Using the equation of state representing phantom energy, $p_r = \omega\rho$ with $\omega < -1$, and taking into account Eqs. (2)-(3), we have the following condition

$$\Phi'(r) = \frac{b + \omega r b'}{2r^2\,(1-b/r)}\,. \tag{5}$$

We now have four equations, namely the field equations, i.e., Eqs. (2)-(4), and Eq. (5), with five unknown functions of r, i.e., $\rho(r)$, $p_r(r)$, $p_t(r)$, $b(r)$ and $\Phi(r)$. To construct solutions with the properties and characteristics of wormholes, we consider restricted choices for $b(r)$ and/or $\Phi(r)$. In cosmology the energy density related to the phantom energy is considered positive, $\rho > 0$, so we shall maintain this condition. This implies that only form functions of the type

$b'(r) > 0$ are allowed. We can construct asymptotically flat spacetimes, in which $b(r)/r \to 0$ and $\Phi \to 0$ as $r \to \infty$. However, one may also construct solutions with a cut-off of the stress-energy, by matching the interior solution to an exterior vacuum spacetime, at a junction interface.

3. SPECIFIC PHANTOM WORMHOLE MODELS

3.1. Asymptotically flat spacetimes

To construct an asymptotically flat wormhole solution [7], consider $\Phi(r) = \Phi_0 = \text{const}$. Thus, from Eq. (5) one obtains

$$b(r) = r_0 (r/r_0)^{-1/\omega}, \tag{6}$$

so that $b(r)/r = (r_0/r)^{(1+\omega)/\omega} \to 0$ for $r \to \infty$. We also verify that $b'(r) = -(1/\omega)(r/r_0)^{-(1+\omega)/\omega}$, so that at the throat the condition $b'(r_0) = 1/|\omega| < 1$ is satisfied.

The stress-energy tensor components are given by

$$p_r(r) = \omega\rho(r) = -\frac{1}{8\pi r_0^2}\left(\frac{r_0}{r}\right)^{3+\frac{1}{\omega}}, \qquad \text{and} \qquad p_t(r) = \frac{1}{16\pi r_0^2}\left(\frac{1+\omega}{\omega}\right)\left(\frac{r_0}{r}\right)^{3+\frac{1}{\omega}}. \tag{7}$$

Thus, determining the parameter ω from observational cosmology, assuming the existence of phantom energy, one may theoretically construct traversable phantom wormholes by considering the above-mentioned form function and a constant redshift function.

Using the "volume integral quantifier", which provides information about the "total amount" of averaged null energy condition (ANEC) violating matter in the spacetime (see Ref. [11] for details), given by $I_V = \int [\rho(r) + p_r(r)]\, dV$, with a cut-off of the stress-energy at a, we have

$$I_V = \int_{r_0}^{a} (r-b)\left[\ln\left(\frac{e^{2\Phi}}{1-b/r}\right)\right]' dr. \tag{8}$$

Considering the specific choices for the form function and redshift function for the traversable wormhole given above, with $\omega = -2$ for simplicity, the volume integral assumes the value $I_V = r_0(1-\sqrt{a/r_0})$. Taking the limit $a \to r_0$, one verifies that $I_V = \int(\rho + p_r)\, dV \to 0$. Thus, as in the examples presented in [11], one may construct a traversable wormhole with arbitrarily small quantities of ANEC violating phantom energy. Although this result is not unexpected it is certainly a fascinating prospect that an advanced civilization may probably construct and sustain a wormhole with vanishing amounts of the material that comprises of approximately 70% of the constitution of the Universe.

3.2. Isotropic pressure

Consider now isotropic pressures, $p_r = p_t = p$. By taking into account the form function, considered above, given by $b(r) = r_0\,(r/r_0)^{-1/\omega}$, and using Eq. (4) and Eq. (2), one finds that the redshift function is given by

$$\Phi(r) = \left(\frac{3\omega+1}{1+\omega}\right)\,\ln\left(\frac{r}{r_0}\right). \tag{9}$$

(See Ref. [7] for details). The stress-energy tensor components are provided by

$$p(r) \quad = \quad \omega\rho(r) = -\frac{1}{8\pi r_0^2}\left(\frac{r_0}{r}\right)^{3+\frac{1}{\omega}}. \tag{10}$$

Note that the spacetime is not asymptotically flat. However, one may match the interior wormhole solution to an exterior vacuum spacetime at a finite junction surface. Using the "volume integral quantifier", Eq. (8), with a cut-off of the stress-energy at a, and taking into account the choices for the form function and redshift function considered above, with $\omega = -2$, the volume integral takes the following value

$$I_V = a\left(1-\sqrt{r_0/a}\right)\,\ln\left[\frac{(a/r_0)^{10}}{1-\sqrt{r_0/a}}\right] + \left(10a + 11r_0 - 21r_0\sqrt{a/r_0}\right) + a\left(\sqrt{r_0/a}-1\right)\,\ln\left[\frac{(a/r_0)^{21/2}}{\sqrt{a/r_0}-1}\right]. \tag{11}$$

Once again taking the limit $a \to r_0$, one verifies that $I_V \to 0$, and as before one may construct a traversable wormhole with arbitrarily small quantities of ANEC violating phantom energy.

4. STABILITY ANALYSIS

4.1. Junction conditions

We shall model specific phantom wormholes by matching an interior traversal wormhole geometry, satisfying the equation of state $p_r = \omega\rho$ with $\omega < -1$, with an exterior Schwarzschild solution at a junction interface Σ, situated outside the event horizon, $a > r_b = 2M$.

Using the Darmois-Israel formalism [12], the surface stress-energy tensor, $S^i{}_j$, at the junction interface Σ, provide us with the following expressions for the surface stresses

$$\sigma = -\frac{1}{4\pi a}\left(\sqrt{1-\frac{2M}{a}+\dot{a}^2}-\sqrt{1-\frac{b(a)}{a}+\dot{a}^2}\right), \tag{12}$$

$$\mathscr{P} = \frac{1}{8\pi a}\left[\frac{1-\frac{M}{a}+\dot{a}^2+a\ddot{a}}{\sqrt{1-\frac{2M}{a}+\dot{a}^2}}-\frac{(1+a\Phi')\left(1-\frac{b}{a}+\dot{a}^2\right)+a\ddot{a}-\frac{\dot{a}^2(b-b'a)}{2(a-b)}}{\sqrt{1-\frac{b(a)}{a}+\dot{a}^2}}\right], \tag{13}$$

where σ and $\mathscr{P}$ are the surface energy density and the tangential surface pressure, respectively (see Refs. ([13, 14, 15]) for details).

We shall use the conservation identity, given by $S^i_{j|i} = \left[T_{\mu\nu}e^{\mu}_{(j)}n^{\nu}\right]^{+}_{-}$, where n^{μ} is the unit normal $4-$vector to Σ, and $e^{\mu}_{(i)}$ are the components of the holonomic basis vectors tangent to Σ. The momentum flux term in the right hand side corresponds to the net discontinuity in the momentum which impinges on the shell. Using $S^i_{\tau|i} = -\left[\dot{\sigma}+2\dot{a}(\sigma+\mathscr{P})/a\right]$, the conservation identity provides us with

$$\sigma' = -\frac{2}{a}(\sigma+\mathscr{P})+\Xi \qquad \text{with} \qquad \Xi = -\frac{1}{4\pi a^2}\left[\frac{b'a-b}{2a\left(1-\frac{b}{a}\right)}+a\Phi'\right]\sqrt{1-\frac{b}{a}+\dot{a}^2}\,. \tag{14}$$

Equation (14) evaluated at a static solution a_0, shall play a fundamental role in determining the stability regions.

Equation (12) may be rearranged to provide the thin shell's equation of motion, i.e., $\dot{a}^2+V(a)=0$, with the potential given by

$$V(a) = F(a)-\left(\frac{m_s}{2a}\right)^2-\left(\frac{aG}{m_s}\right)^2, \tag{15}$$

where $m_s = 4\pi\sigma a^2$ is the surface mass of the thin shell. For computational purposes and notational convenience, we define the following factors

$$F(a) = 1-\frac{b(a)/2+M}{a} \qquad \text{and} \qquad G(a) = \frac{M-b(a)/2}{a}, \tag{16}$$

Linearizing around a stable solution situated at a_0, we consider a Taylor expansion of $V(a)$ around a_0 to second order, given by

$$V(a) = V(a_0)+V'(a_0)(a-a_0)+\frac{1}{2}V''(a_0)(a-a_0)^2+O[(a-a_0)^3]\,. \tag{17}$$

Evaluated at the static solution, at $a=a_0$, we verify that $V(a_0)=0$ and $V'(a_0)=0$. From the condition $V'(a_0)=0$, one extracts the following useful equilibrium relationship

$$\Gamma \equiv \left(\frac{m_s}{2a_0}\right)' = \left(\frac{a_0}{m_s}\right)\left[F'-2\left(\frac{a_0G}{m_s}\right)\left(\frac{a_0G}{m_s}\right)'\right], \tag{18}$$

which will be used in determining the master equation, responsible for dictating the stable equilibrium configurations.

The solution is stable if and only if $V(a)$ has a local minimum at a_0 and $V''(a_0) > 0$ is verified. The latter condition takes the form

$$\left(\frac{m_s}{2a}\right)\left(\frac{m_s}{2a}\right)'' < \Psi - \Gamma^2, \qquad \text{with} \qquad \Psi = \frac{F''}{2} - \left[\left(\frac{aG}{m_s}\right)'\right]^2 - \left(\frac{aG}{m_s}\right)\left(\frac{aG}{m_s}\right)''. \tag{19}$$

Using $m_s = 4\pi a^2\sigma$, and taking into account the radial derivative of σ', Eq. (14) can be rearranged to provide the following relationship

$$\left(\frac{m_s}{2a}\right)'' = \Upsilon - 4\pi\sigma'\eta\,, \qquad \text{with} \qquad \Upsilon \equiv \frac{4\pi}{a}\left(\sigma + \mathscr{P}\right) + 2\pi a\,\Xi'\,, \tag{20}$$

and the parameter η is defined as $\eta = \mathscr{P}'/\sigma'$.

Equation (20) will play a fundamental role in determining the stability regions of the respective solutions. Note that the parameter $\sqrt{\eta}$ is normally interpreted as the speed of sound, so that one would expect that $0 < \eta \leq 1$, based on the requirement that the speed of sound should not exceed the speed of light. However, in the presence of exotic matter this cannot naively de done so. Therefore, in this work the above range will be relaxed. We refer the reader to Ref. [9] for an extensive discussion on the respective physical interpretation of η in the presence of exotic matter.

We shall use η as a parametrization of the stable equilibrium, so that there is no need to specify a surface equation of state. Thus, substituting Eq. (20) into Eq. (19), one deduces the master equation given by

$$\sigma' m_s \eta_0 > \Theta\,, \qquad \text{with} \qquad \Theta \equiv \frac{a_0}{2\pi}\left(\Gamma^2 - \Psi\right) + \frac{1}{4\pi} m_s \Upsilon\,, \tag{21}$$

and $\eta_0 = \eta(a_0)$. The master equation dictate stable equilibrium regions, given by the following inequalities

$$\eta_0 > \overline{\Theta}, \qquad \text{if} \qquad \sigma' m_s > 0\,, \tag{22}$$

$$\eta_0 < \overline{\Theta}, \qquad \text{if} \qquad \sigma' m_s < 0\,, \tag{23}$$

with the definition $\overline{\Theta} \equiv \Theta/(\sigma' m_s)$.

We shall now consider the phantom wormhole geometries found in Secion 3, and consequently determine the stability regions dictated by the inequalities (22)-(23). In the specific cases that follow, the explicit form of Υ, Ψ, Θ and $\overline{\Theta}$ are extremely messy, so that as in [10], we find it more instructive to show the stability regions graphically.

4.2. Stability regions

4.2.1. Asymptotically flat spacetimes

Consider the specific choices for the redshift and form functions, for an asymptotically flat spacetime, given by $\Phi(r) = \Phi_0 = \text{const}$ and the form function given by Eq. (6), $b(r) = r_0(r/r_0)^{-1/\omega}$. To determine the stability regions of this solution, we shall separate the cases of $b(a_0) < 2M$ and $b(a_0) > 2M$. From Eq. (12) and the definition of $m_s = 4\pi a_0^2\sigma$, this corresponds to $m_s > 0$ and $m_s < 0$, respectively. Here, we shall relax the condition that the surface energy density be positive, as in considering traversable wormhole geometries, one is already dealing with exotic matter. Note that for $\sigma < 0$, the weak energy condition is readily violated.

For $b(a_0) < 2M$, i.e., for a positive surface energy density, we need to impose the condition $r_0 < 2M$, so that the junction radius lies outside the event horizon, $a_0 > 2M$. Thus, the junction radius lies in the following range

$$2M < a_0 < 2M\left(2M/r_0\right)^{-(1+\omega)}\,. \tag{24}$$

For a fixed value of ω, we verify that as $r_0 \to 0$, then $a_0 \to \infty$. The range decreases, i.e., $a_0 \to 2M$, as $r_0 \to 2M$. Note that by fixing r_0 and decreasing ω, the range of a_0 is also significantly increased.

For a fixed value of the parameter, for instance $\omega = -2$, we shall consider the following cases: $r_0/M = 1.0$, so that $2 < a_0/M < 4$; and for $r_0/M = 0.25$, we have $2 < a_0/M < 16$. The respective stability regions are depicted in Fig. 1. From Eq. (14), one may show that $\sigma' < 0$, and as $\sigma > 0$, this implies $m_s\sigma' < 0$. Thus, the stability regions, dictated

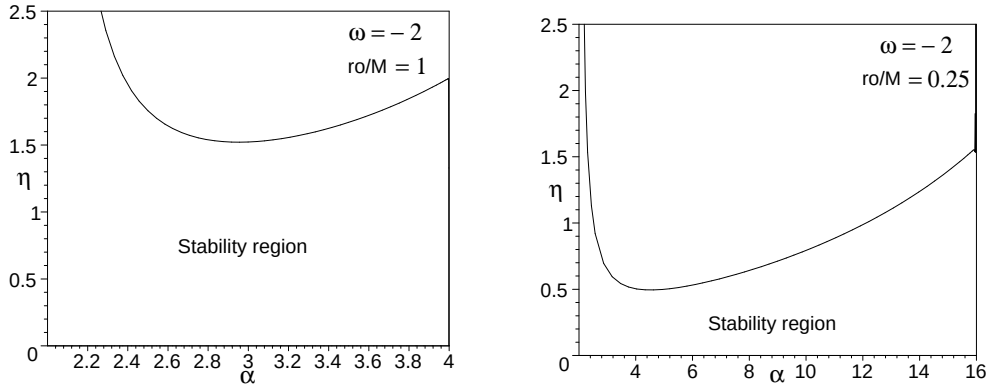

FIGURE 1. Plots for a positive surface energy density, i.e., $b(a_0) < 2M$. We have defined $\alpha = a_0/M$, and considered $\omega = -2$ for both cases. The first plot is given by $r_0/M = 1$, and the second by $r_0/M = 0.25$. The stability regions are given below the solid curve. See the text for details.

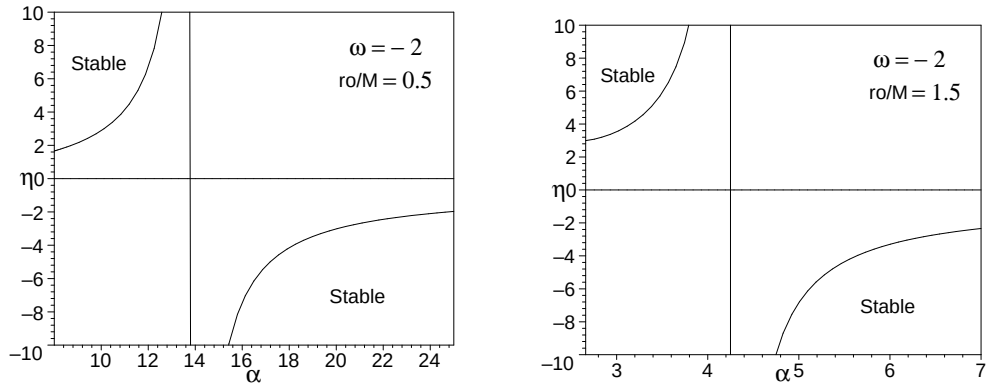

FIGURE 2. Plots for a negative surface energy density, considering $r_0/M < 2$. We have defined $\alpha = a_0/M$, and considered $\omega = -2$ for both cases. The first plot is given by $r_0/M = 0.5$, and the second by $r_0/M = 1.5$. The stability regions are given above the first solid curve, and below the second solid curve. See the text for details.

by the inequality (23), lie beneath the solid lines in the plots of Fig. 1. For decreasing values of r_0/M, as a_0 increases, the values of η_0 are further restricted. Using positive surface energy densities, stable geometries may be found well within the bound of $0 < \eta_0 \leq 1$, and the stability regions increase for increasing values of r_0/M.

For $b(a_0) > 2M$, the surface mass of the thin shell is negative, $m_s(a_0) < 0$. We shall separate the cases of $r_0 < 2M$ and $r_0 > 2M$. If $r_0 < 2M$, the range of the junction radius is given by $a_0 > 2M\,(2M/r_0)^{-(1+\omega)}$. For this specific case, σ' possesses one real positive root, R, in the above range, signalling the presence of an asymptote, $\sigma'|_R = 0$. We verify that $\sigma' < 0$ for $2M(2M/r_0)^{-(1+\omega)} < a_0 < R$, and $\sigma' > 0$ for $a_0 > R$. Thus, the stability regions are given by

$$\eta_0 \;>\; \overline{\Theta}, \quad \text{if} \quad 2M\,(2M/r_0)^{-(1+\omega)} < a_0 < R, \tag{25}$$

$$\eta_0 \;<\; \overline{\Theta}, \quad \text{if} \quad a_0 > R. \tag{26}$$

Consider for $\omega = -2$, the particular cases of $r_0/M = 0.5$, so that $a_0/M > 8$, and $r_0/M = 1.5$, so that $a_0/M > 2.667$. The asymptotes, $\sigma'|_R = 0$, for these cases exist at $R/M \simeq 13.9$ and $R/M \simeq 4.24$, respectively. These cases are represented in Fig. 2. Note that for increasing values of r_0/M, the range of a_0 decreases, and the values of η_0 are less restricted. Thus, one may conclude that the stability regions increase, for increasing values of r_0/M.

If $r_0 > 2M$, then obviously $a_0 > r_0$. We verify that $\sigma' > 0$, and consequently $m_s\,\sigma' < 0$, so that the stability region is given by inequality (23). We verify that the values of η_0 are always negative. However, by increasing r_0/M, the values of η_0 become less restricted, and the range of a_0 decreases.

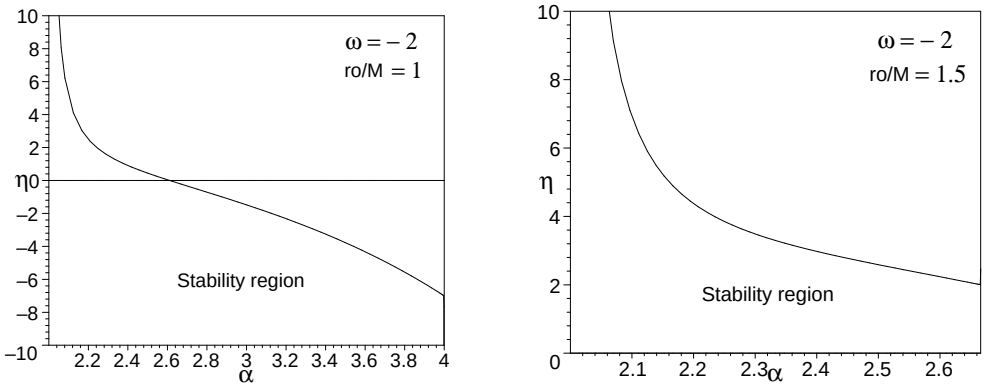

FIGURE 3. Plots for an isotropic pressure phantom wormhole. We have defined $\alpha = a_0/M$ and considered $\omega = -2$ for both cases. For $b(a_0) < 2M$, the condition $r_0 < 2M$ is imposed. The first plot is given by $r_0/M = 1.0$, and the second by $r_0/M = 1.5$. The stability regions are given below the solid curves.

4.2.2. Isotropic pressure, $p_r = p_t = p$

Consider an isotropic pressure phantom wormhole geometry, with the redshift function given by Eq. (9), $\Phi(r) = (3\omega+1)/(1+\omega)\,\ln(r/r_0)$ and $b(r) = r_0\,(r/r_0)^{-1/\omega}$. To determine the stability regions of this solution, as in the previous case, we shall separate the cases of $b(a_0) < 2M$ and $b(a_0) > 2M$.

For $b(a_0) < 2M$, we have $m_s > 0$, and the condition $r_0 < 2M$ is imposed. Therefore, the junction radius lies in the same range as the previous case, i.e., Eq. (24). We also verify that $\sigma' < 0$ in the respective range. Thus the stability region is given by

$$\eta_0 < \overline{\Theta}, \quad \text{if} \quad 2M < a_0 < 2M\,(2M/r_0)^{-(1+\omega)}\,. \tag{27}$$

Consider, for simplicity, $\omega = -2$, and the cases for $r_0/M = 1$ and $r_0/M = 1.5$ are analyzed in Fig. 3. The ranges are given by $2 < a_0/M < 4$ and $2 < a_0/M < 2.667$, respectively. Note that as r_0/M decreases, the range of a_0 increases. However, the values of the parameter η_0 become more restricted. Thus, one may conclude that the stability regions increase, as r_0/M increases.

For $b(a_0) > 2M$, then $m_s(a_0) < 0$. As before, we shall separate the cases of $r_0 < 2M$ and $r_0 > 2M$. For $r_0 < 2M$, the range of a_0 is given by $a_0 > 2M(2M/r_0)^{-(1+\omega)}$, as in the previous case of the asymptotically flat wormhole spacetime.

For this case σ' also possesses one real positive root, R, in the respective range. We have $\sigma' < 0$ for $(2M/r_0)^{-1/\omega} < a < R$, and $\sigma' > 0$ for $a_0 > R$. The stability regions are also given by the conditions (25)-(26). We have considered the specific cases of $r_0/M = 1$ so that the respective range is $a_0/M > 4$; and $r_0/M = 1.5$, so that $a_0/M > 2.667$. The asymptotes, $\sigma'|_R = 0$, for these cases exist at $R/M \simeq 6.72$ and $R/M \simeq 4.24$, respectively. This analysis is depicted in the plots of Fig. 4. For decreasing values of r_0/M, the stability parameter η_0 becomes less restricted and the range of the junction radius increases. Thus, one may conclude that the stability regions increase for decreasing values of r_0/M.

5. CONCLUSION

As the Universe is probably constituted of approximately 70% of null energy condition violating phantom energy, this cosmic fluid may be used as a possible source to theoretically construct traversable wormholes. In fact, it was found that infinitesimal amounts of phantom energy may support traversable wormholes [7]. In this paper, we have modelled phantom wormholes by matching an interior traversable wormhole geometry, satisfying the equation of state $p = \omega\rho$ with $\omega < -1$, to an exterior vacuum solution at a finite junction interface. We have analyzed the stability of these phantom wormholes, an issue of fundamental importance, to linearized perturbations around static solutions, by including the momentum flux term in the conservation identity. We have considered two particularly interesting cases, namely, that of an asymptotically flat spacetime, and that of an isotropic pressure wormhole geometry. We have separated the cases of positive and negative surface energy densities and found that the stable equilibrium regions may be significantly increased by strategically varying the wormhole throat. As we are considering exotic matter, we have relaxed the condition $0 < \eta_0 \leq 1$, and found stability regions for phantom wormholes well beyond this range.

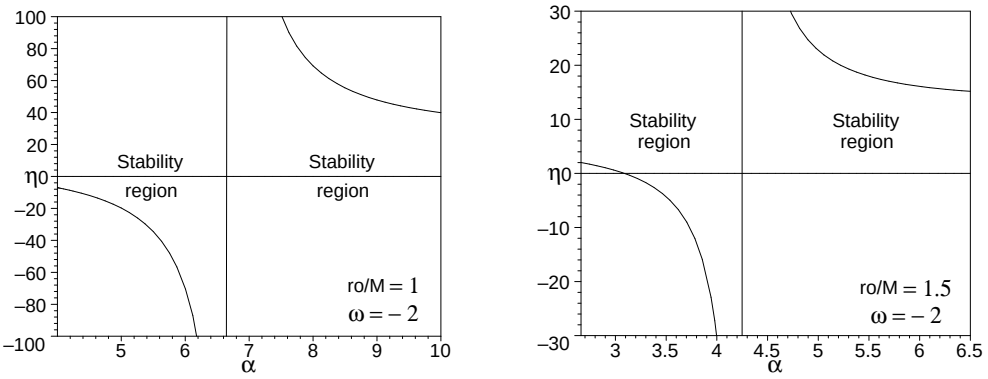

FIGURE 4. Plots for an isotropic pressure phantom wormhole, for $b(a_0) > 2M$ and $r_0 < 2M$. We have defined $\alpha = a_0/M$ and considered $\omega = -2$ for both cases. The first plot is given by $r_0/M = 1.0$, and the second by $r_0/M = 1.5$. The stability regions are given above the first solid curve, and below the second solid curve.

An interesting feature of the phantom regime is that due to the fact of the accelerated expansion of the Universe, macroscopic wormholes could naturally be grown from the submicroscopic constructions that originally pervaded the quantum foam [16]. The accretion of phantom energy onto Morris-Thorne wormholes was further explored in Refs. [17], and it was shown that this accretion gradually increases the wormhole throat which eventually overtakes the accelerated expansion of the universe, consequently engulfing the entire Universe, and becomes infinite at a time in the future before the big rip. This process was dubbed the "Big Trip" [17]. Traversable wormholes supported by the generalized Chaplygin gas were also found [18], and in the context of the "Big Trip", it was found that the latter may be avoided in a wide region of the Chaplygin parameters, by the accretion of a generalized Chaplygin gas onto wormholes [19]. In concluding, it is noteworthy the relative ease with which one may theoretically construct traversable wormholes with the exotic fluid equations of state used in cosmology to explain the present accelerated expansion of the Universe.

REFERENCES

1. A. Grant *et al*, Astrophys. J. **560** 49-71 (2001); S. Perlmutter, M. S. Turner and M. White, Phys. Rev. Lett. **83** 670-673 (1999); C. L. Bennett *et al*, Astrophys. J. Suppl. **148** 1 (2003); G. Hinshaw *et al*, Astrophys. J. Suppl. **148** 135 (2003).
2. R. R. Caldwell, M. Kamionkowski and N. N. Weinberg, Phys. Rev. Lett. **91** 071301 (2003) [arXiv:astro-ph/0302506].
3. Z. Guo, Y. Piao, X. Zhang and Y. Zhang, Phys. Lett. **B608** 177-182 (2005); L. Perivolaropoulos, Phys.Rev. D **71** 063503 (2005); H. Wei and R. G. Cai, Class. Quant. Grav. **22** 3189-3202 (2005); H. Stefancic, Phys. Rev. D **71** 124036 (2005).
4. M. Morris and K.S. Thorne, Am. J. Phys. **56**, 395 (1988).
5. Visser M 1995 *Lorentzian Wormholes: From Einstein to Hawking* (American Institute of Physics, New York)
6. S. Sushkov, Phys. Rev. D **71**, 043520 (2005).
7. F. S. N. Lobo, Phys. Rev. D **71**, 084011 (2005).
8. F. S. N. Lobo, Class. Quant. Grav. **21** 4811 (2004); J. P. S. Lemos, F. S. N. Lobo and S. Q. de Oliveira, Phys. Rev. D **68**, 064004 (2003); F. S. N. Lobo, Gen. Rel. Grav. **37** 2023-2038 (2005); J. P. S. Lemos and F. S. N. Lobo, Phys. Rev. D **69** (2004) 104007.
9. E. Poisson and M. Visser, Phys. Rev. D **52** 7318 (1995); E. F. Eiroa and G. E. Romero, Gen. Rel. Grav. **36**, 651 (2004); F. S. N. Lobo and P. Crawford, Class. Quant. Grav. **21**, 391 (2004).
10. M. Ishak and K. Lake, Phys. Rev. D **65** 044011 (2002).
11. M. Visser, S. Kar and N. Dadhich, Phys. Rev. Lett. **90**, 201102 (2003).
12. W. Israel, Nuovo Cimento **44**B, 1 (1966); and corrections in *ibid.* **48**B, 463 (1966).
13. F. S. N. Lobo, Phys. Rev. D **71**, 124022 (2005).
14. F. S. N. Lobo, Class. Quant. Grav. **23**, 1525-1541 (2006).
15. F. S. N. Lobo and P. Crawford, Class. Quant. Grav. **22**, 4869 (2005).
16. P. F. González-Díaz, Phys. Rev. D **68**, 084016 (2003).
17. P. F. González-Díaz, Phys. Rev. Lett. **93** 071301 (2004); P. F. González-Díaz, Phys. Lett. **B632**, 159-161 (2006).
18. F. S. N. Lobo, Phys. Rev. **D** 73, 064028 (2006).
19. J. A. Jiménez Madrid, Phys. Lett. **B634** 106 (2006).